Article

A sentinel watching over inter-tidal seagrass phenology across Western Europe and North Africa

Check for updates

Bede Ffinian Rowe Davies [1] ✉, Simon Oiry[1], Philippe Rosa[1], Maria Laura Zoffoli[2], Ana I. Sousa [3], Oliver R. Thomas [4], Dan A. Smale [5], Melanie C. Austen [4], Lauren Biermann[4], Martin J. Attrill [4,6], Alejandro Roman [7], Gabriel Navarro [7], Anne-Laure Barillé[8], Nicolas Harin[8], Daniel Clewley[9], Victor Martinez-Vicente [9], Pierre Gernez [1] & Laurent Barillé[1]

Seagrasses are marine flowering plants that form extensive meadows from the inter-tidal zone up to ~50 m depth. As biological and ecological Essential Biodiversity Variables, seagrass cover and composition provide a wide range of ecosystem services. Inter-tidal seagrass meadows provide services to many ecosystems, so monitoring their occurrence, extent, condition and diversity can be used to indicate the biodiversity and health of local ecosystems. Current global estimates of seagrass extent and recent reviews either do not mention inter-tidal seagrasses and their seasonal variation, or combine them with sub-tidal seagrasses. Here, using high-spatial and high-temporal resolution satellite data (Sentinel-2), we demonstrate a method for consistently mapping inter-tidal seagrass meadows and their phenology at a continental scale. We were able to highlight varying seasonal patterns that are observable across a 23° latitudinal range. Timings of peaks in seagrass extent varied by up to 5 months, rather than the previously assumed marginal to non-existent variation in peak timing. These results will aid management by providing high-resolution spatio-temporal monitoring data to better inform seagrass conservation and restoration. They also highlight the high level of seasonal variability in inter-tidal seagrass, meaning combination with sub-tidal seagrass for global assessments will likely produce misleading or incorrect estimates.

Seagrasses, a group of flowering marine plants, can form extensive inter and sub-tidal meadows ranging across all continents except Antarctica. These habitats have significant ecological and socioeconomic value[1,2] by providing key forage, refuge and nursery habitats for fisheries species and non-targeted species[3–5]; supporting tourism and recreation; climate regulation through carbon sequestration[6]; coastal stabilisation[7] and water quality mediation[8]. It is estimated that, globally, hundreds of millions of people rely upon seagrass habitats for the benefits they provide through food provisioning and livelihoods[4]. Yet, seagrass habitats are under increasing pressure from direct and indirect anthropogenic impacts, from local to regional scales[9]. Many of the effects of human pressures, including climate change, will be felt acutely

by seagrass habitats within the inter-tidal zone. This is already happening thanks to their exposure to both aquatic and atmospheric climatic events, vulnerability to sea level change, close proximity to effluent runoff, pollution and eutrophication from anthropogenic sources and their spatial overlap with coastal development and aquaculture[10–12].

To effectively and sustainably manage seagrass ecosystems, protect and maximise the services they underpin, and safeguard against future human-mediated impacts, we first require an understanding of ecosystem extent, and how this may change over different spatio-temporal scales. However, there are large uncertainties around regional and global estimates of seagrass coverage, which are the baseline requirements for assessments of the

[1]Nantes Université, Institut des Substances et Organismes de la Mer, ISOMer, UR2160, Nantes, F-44000, France. [2]Consiglio Nazionale delle Riecerche, Instituto di Science Marine (CNR-ISMAR), Rome, Italy. [3]ECOMARE–Laboratory for Innovation and Sustainability of Marine Biological Resources, CESAM–Centre for Environmental and Marine Studies, Department of Biology, University of Aveiro, Campus Universitário de Santiago, Aveiro, Portugal. [4]School of Biological and Marine Science, University of Plymouth, Plymouth, PL4 8AA, UK. [5]Marine Biological Association of the UK, Citadel Hill, Plymouth, PL1 2PB, UK. [6]Ocean Conservation Trust, Rope Walk, Coxside, Plymouth, PL4 0LF, UK. [7]Institute of Marine Sciences of Andalusia (ICMAN-CSIC), Spanish National Research Council (CSIC), Department of Ecology and Coastal Management, 11510 Puerto Real, Spain. [8]Bio-littoral, Faculté des Sciences et des Techniques, B.P. 92208, 44322 Nantes, France. [9]Plymouth Marine Laboratory, Prospect Place, The Hoe, Plymouth, UK. ✉e-mail: bedeffinian@gmail.com

ecological goods and services they provide[13,14]. Within global efforts to tackle climate change, significant emphasis is being put on conservation, restoration and expansion of Blue Carbon (BC) ecosystems, such as seagrasses[15]. Restoration projects could benefit from quantifying past trajectories of seagrass bed extent and phenology at a high temporal resolution. However, regular mapping is still lacking for most inter-tidal seagrasses.

The first step to assessing variability in inter-tidal seagrass meadows is to develop accurate, robust, repeatable and cost-effective approaches to monitoring these habitats over appropriate spatial and temporal scales. Earth observation (EO) with satellite imagery has been suggested to supplement traditional monitoring of habitats at large spatial scales and near real-time[16]. Optical remote sensing, depending on the sensor being used, provides reflectance of incident sunlight across visible and near-infra-red wavelengths, with certain wavelengths being used to estimate the percentage cover or productivity of vegetation[17]. This approach has been used to assess inter-annual variation of known monospecific seagrass meadows[5,17–19]. Different pigments and structures absorb and reflect specific wavelengths differently[20], thus inter-tidal vegetation types can be discriminated by their spectral reflectance signature[21,22]. However, similarly pigmented classes, such as seagrasses and some macroalgae (e.g. Ulvophyceae), have created confusion when mapping vegetation through remote sensing[16]. Yet, efforts that make use of more complex classification methods, such as machine and deep learning, have shown the potential to distinguish different inter-tidal habitats from Sentinel-2 data with high accuracy, specifically seagrass[23], thus opening new perspectives for inter-tidal seagrass mapping from space.

Contrary to sub-tidal seagrass meadows, which have been mapped at continental scales[24], inter-tidal meadows have rarely been mapped at scales larger than a single bay or estuary, and never at the continental scale. This has led to gaps and uncertainties in global inter-tidal seagrass estimations. Specifically, there is a distinct lack of monitoring of the temporal variation in extent and distribution, such as long-term trajectories or inter-annual phenology. Across the North-East Atlantic, climatological conditions, such as temperature and light levels, and hydrodynamic processes vary markedly across seasons and regions, affecting the phenology of inter-tidal seagrass. Previous studies have examined seasonality in inter-tidal seagrass populations with in situ measurements[6,25–28]. When Northern European inter-tidal seagrass meadows have been assessed, the peak in seasonal growth has been assumed to vary minimally around summer months, even across 20° latitude[29,30]. Determining the period of 'peak' growth or 'peak' extent is therefore fundamental for standardising the measurement of seagrass morphometrics and density across a latitudinal range[29–33]. Seasonal growth patterns and retreat of above-ground extent need to be understood, considering local-to-regional variability in phenology. This will be essential for effectively monitoring inter-tidal seagrasses as they continue to be affected by anthropogenic pressures, such as localised disturbances and global climate change.

Previous attempts to analyse latitudinal trends in the seasonality of seagrass biomass either concerned sub-tidal seagrass[34], or were limited by the scarcity and/or too coarse spatio-temporal resolution of available data[35,36]. Here, we built a neural network model to provide, for the first time, a synoptic mapping of inter-tidal seagrass cover and extent using high-resolution EO at a continental scale: the Intertidal Classification of Europe: Categorising Reflectance of Emerged Areas of Marine vegetation with Sentinel-2 (ICE CREAMS) model. We validated and applied our model to 12 inter-tidal seagrass meadows seasonally across 7 years, using almost 800 Sentienl-2 (S2) images, spanning 23° latitude from Morocco to Scotland. Our results made it possible to analyse the latitudinal changes in inter-tidal seagrass phenology in Europe. Our hypotheses were twofold: (1) The seasonality of inter-tidal seagrass shows a clear latitudinal trend, similar to that of terrestrial grass[37] and sub-tidal seagrass[34]; (2) temporal variations in inter-tidal seagrass are expected to be dictated by a myriad of biotic and abiotic local environmental drivers; however, latitude-dependent changes are expected to be driven by broad-scale changes in climate-related parameters such as air temperature and solar irradiance.

Results and discussion
Seagrass phenology across North-East Atlantic
We developed a two-step process to accurately and robustly assess the extent of inter-tidal seagrass across continental scales from Sentinel-2 imagery, and quantify seasonal variability. First, we classified inter-tidal habitats into 9 classes (bare sand, bare mud, seagrass, microphytobenthos, green macroalgae, brown macroalgae, yellow-green macroalgae, and water) using a deep learning Neural Network classifier: the ICE CREAMS model. Our classifier was extensively trained across sites and habitat types using very high-resolution (8 mm) multispectral drone imagery and in situ observations. Second, the Normalised Difference Vegetation Index (NDVI) was computed for each seagrass pixel and converted into Seagrass Percentage Cover using a previously validated algorithm[19]. The predicted seagrass classification was validated using ~12,000 S2 pixels collated across 6 sites in Europe from the Tamar Estuary (England) to Cádiz Bay (Spain). Validation data, which were independent of training data, came from a combination of very high spatial resolution, photo-interpreted drone imagery and georeferenced photo-quadrats (0.25 m^2), with the classification of inter-tidal habitat being aggregated (most frequent class) at the S2 spatial resolution. This was then compared to concomitant low-tide, cloud-free S2 imagery. The ICE CREAMS model validation of the binary presence or absence of seagrass gave an overall global accuracy of 0.82. In particular, our model was highly successful in distinguishing seagrass from green macroalgae because we used the full spectral potential of Sentinel-2 (i.e. 10 bands in the visible and near-infrared spectral domains), which was previously demonstrated to reach an accuracy of 95% to classify these two classes[23]. All low tide, cloud-free Sentinel-2 imagery from 2017 to 2023 were then processed to provide habitat classification at the 10 m resolution and compute time-series of inter-tidal seagrass extent for 12 known inter-tidal seagrass meadows across Western Europe and Northern Africa.

Across our sites, which ranged from Morocco to Scotland, covering ~23° of latitude (Fig. 1), strikingly different seasonal patterns in cumulative inter-tidal seagrass cover were found, with strong maxima and minima in the northern sites (maxima of ~10 km^2 down to 0 km^2 minima in the German site), while sites in Spain, Portugal and Morocco appeared to show smaller amplitude in their seasonal cycle (Fig. 2: maxima of ~1.5 km^2 down to ~0.9 km^2 minima in Cádiz Bay). Furthermore, the maxima and minima occurred later in the year at the more southerly sites (Figs. 2 and 3). Timing of maximum extent ranges from late August to late September in latitudes above 45°, while below this latitude, maximum extent occurs from November through to late January. Timings and ranges of minimum extent are more spread out, with most northern sites having their minimum from January to May. All of the more southern sites had minima from June to early August, with the exceptions of Santander Bay and the Tagus Estuary, which occurred from March to May.

The relative magnitude of minima is considerably greater in the north, with extensive periods of close-to-zero seagrass cover, while the southern sites rarely reach zero covers at any point during the year, even at their minimum levels (e.g. Fig. 4). Likewise, the duration of these minimum seagrass covers generally last longer in the northern sites (Fig. 3).

As these northern sites are ranging from much lower seagrass covers up to their maximum in extent, their growth rate is proportionally higher (Fig. 2). Maximum growth rates, and subsequent declines, of northern sites tend to be far higher than southern rates, with the highest growth rate in the north (~ 0.2 km^2 w^{-1} in the German site) being ~26 times greater than the highest growth rate in the south (~ 0.0075 km^2 w^{-1} in the Moroccan site).

Drivers of seagrass phenology
Clear differences in seasonality were shown across the 23° assessed, with changes in timing and magnitude of extent maxima and minima, as well as growth rates. The range in timing of maxima from the most northern site to the most southern site is from late August to early February (5 months). This is contrary to many assertions that the timing of maximum inter-tidal seagrass extent in Europe ranges from late July to early September (only 2 months)[29,30] or even occurring at the same time throughout the whole

Fig. 1 | Inter-Tidal Seagrass meadows. Sites selected to analyse the phenology of inter-tidal seagrass across the North-East Atlantic.
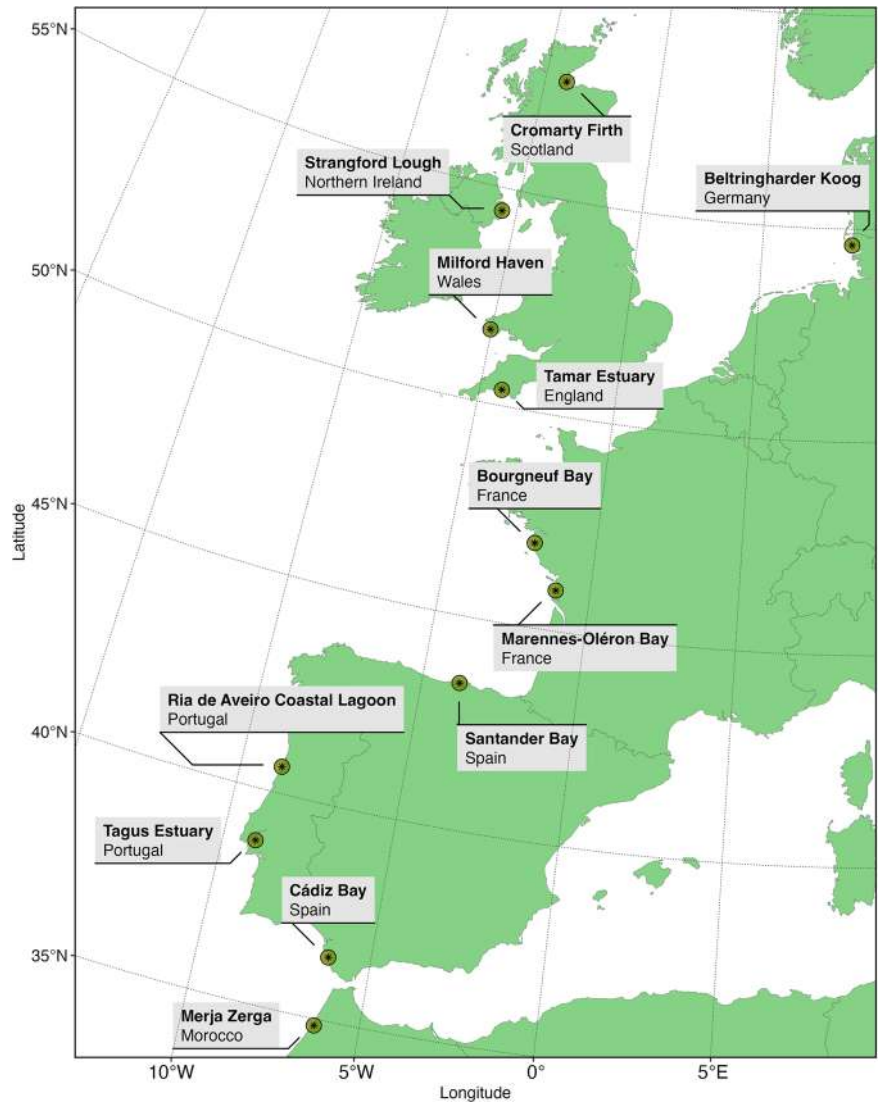
North-East Atlantic. The seagrass extent variability was more critical at higher latitudes, as previously reported[35]. While latitude seemed to drive seagrass phenology, there were more complex patterns of influence shown by the Temperature and Direct Solar radiation (Fig. 3b). A negative effect of solar radiation was found across all latitudes, particularly south of 50°N. An interpretation of this counter-intuitive effect of solar irradiance on seagrass extent is that increased light radiation would lead to a higher chance of desiccation in the southern sites. The temperature had a positive effect in most northern sites, the exception being Cromarty Firth at 57.6°N, but was negligible from 40.7°N (Ria de Aveiro Coastal Lagoon) or negative (Cádiz Bay). It is likely that many different abiotic and biotic factors, both regionally and locally, influence the timing and magnitude of seagrass seasonal phenology. While not assessed here, the effects of nutrients, pollution, physical disturbance, tidal regime, local topography and tidal timing will be highly influential on inter-tidal seagrass phenology. To assess the effects of these factors on seagrass extent, the underlying patterns of seagrass phenology need to be understood, yet many authors have highlighted the lack of up-to-date inter-tidal seagrass phenology data that effectively cover both inter- and intra-annual variation[9,38–40].

### Earth observation at the continental scale
This work constitutes the first assessment of inter-tidal seagrass phenology applying a consistent methodology across a continental scale, spanning 12 sites of the North-East Atlantic (over 23° of latitude), utilising 7 years of

Sentinel-2 multispectral imagery (~800 images). The use of EO, and specifically high-spatial resolution multispectral remote sensing, to map and assess sub- and inter-tidal habitats has increased in recent years, with many studies assessing local to global trends in habitats[5,19,22,41–44]. This increase in global scale monitoring has been aided in the availability of free-to-use cloud-based parallel-processing tools, such as Google Earth Engine[45]. However, there are many technical and practical considerations still inherent to EO, such as spatial, temporal and spectral resolution, data access, processing and computing capability[16], where assessment objective will dictate the choice of the sensor and the processing pipeline, by prioritising certain elements over others.

General limitations
Within the current method, certain assumptions have been made that need to be considered. Firstly, low NDVI and Seagrass Percentage Cover pixels (below 0.25 NDVI, ~20% SPC) were removed from the analysis, meaning some areas of low inter-tidal seagrass cover may have been missed with potential underestimation of cumulative seagrass cover. It has also been noted that seasonal variation in pigment composition of inter-tidal seagrass may influence the relationship between SPC and NDVI[19], although Chlorophyll *a* concentration, which NDVI is a proxy for, varies minimally[46]. NDVI has been shown to correspond non-linearly with vegetation cover at high values (>0.75), but the maximum NDVI value used for conversion to SPC was 0.71. Furthermore, using NDVI to convert to SPC has a saturation
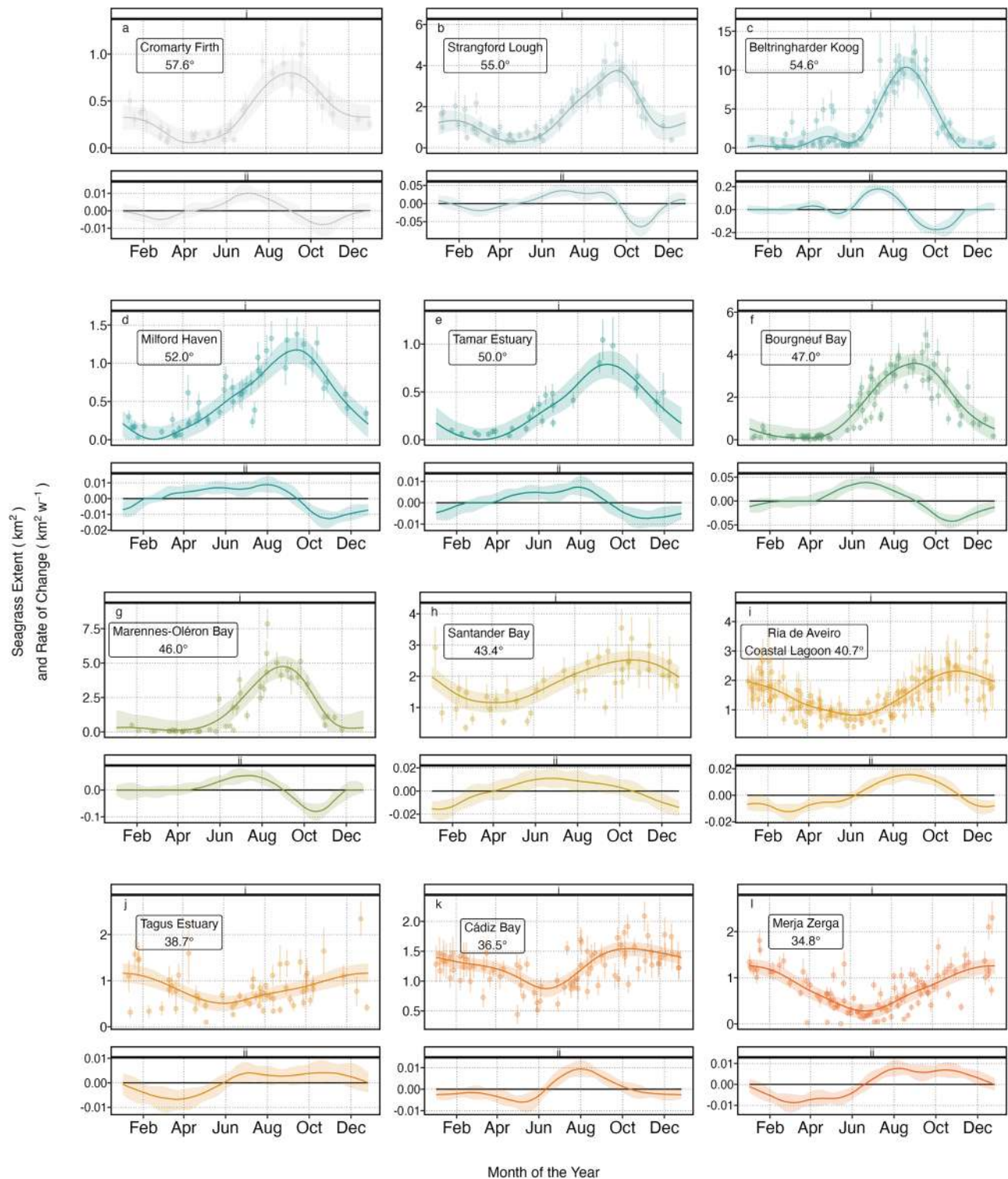
Fig. 2 | Inter-Tidal Seagrass Extent over time. Seasonal change in cumulative seagrass cover in km^2 (i) and rate of change in cumulative seagrass cover in km^2 w^{-1} (ii) across 12 seagrass meadows spanning 23° of latitude. Panels show different sites as labelled: **a** Cromarty Firth; **b** Strangford Lough; **c** Beltringharder Koog; **d** Milford Haven; **e** Tamar Estuary; **f** Bourgneuf Bay; **g** Marennes-Oléron; **h** Santander Bay; **i** Ria de Aveiro Coastal Lagoon; **j** Tagus Estuary; **k** Cádiz Bay and **l** Merja Zerga. Points with error bars show neural network estimated cumulative cover and average uncertainty per satellite image, while the dark line and shading show median and 89% confidence intervals. Plot labels show the site and its latitude (in degrees).

level, where increased seagrass density when already at 100% (0.71 NDVI) will stay at 100% regardless of potentially large differences in seagrass biomass. Lastly, drifting macroalgae (Ulvophyceae and Rhodophyceae) during low tide may cover areas of seagrass meadows, which may also lead to seagrass extent underestimation.

Specific limitations and advantages
Here, Sentinel-2, using 12 spectral bands at 10 m resolution (low spatial resolution bands resampled to 10 m), allowed free access to 7 years of atmospherically corrected imagery, with a revisit time of 3–5 days since the launch of S2B to complement S2A in 2017, meaning seasonal variability was
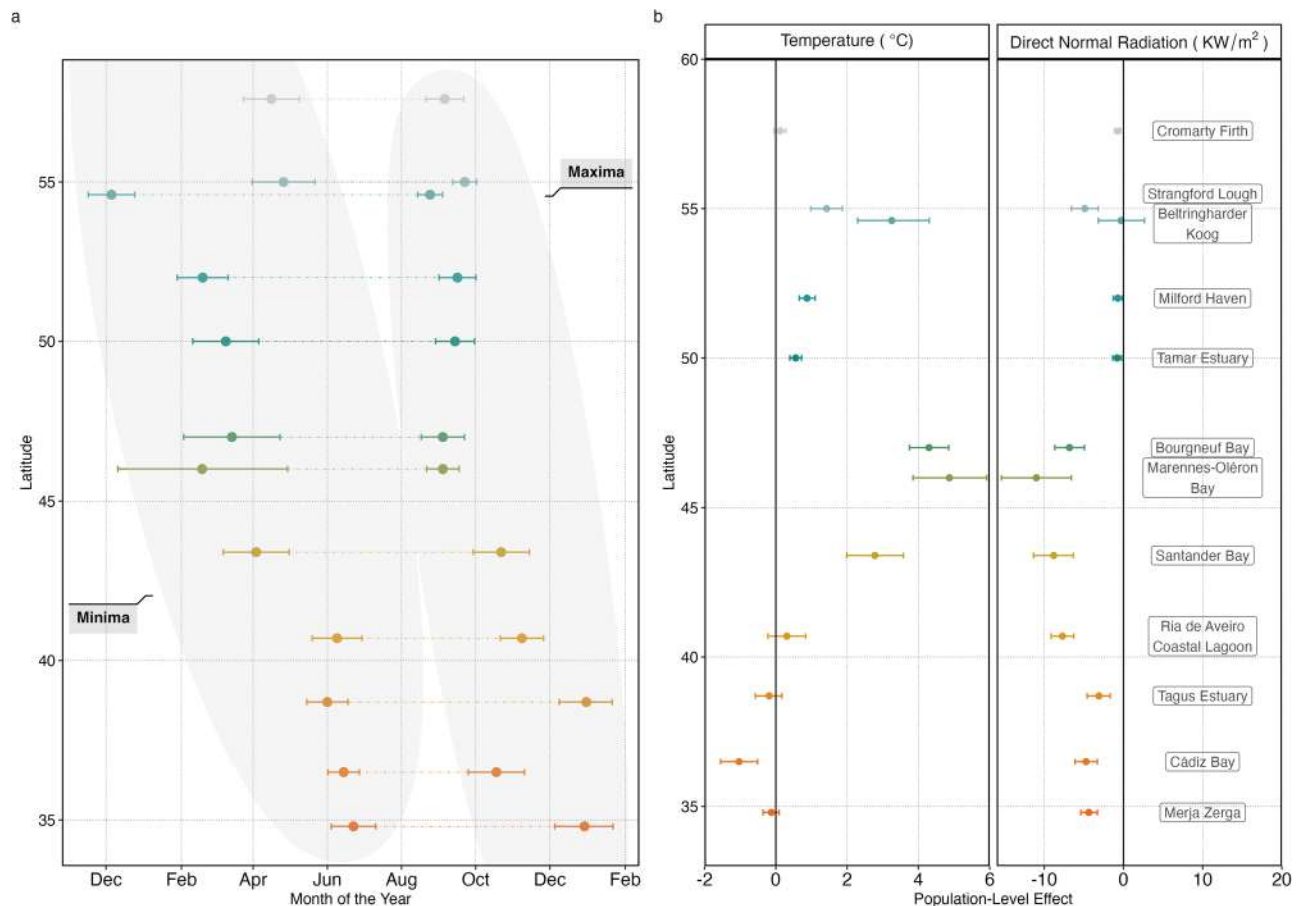
Fig. 3 | Inter-Tidal Phenology Events and Effects of Environmental Drivers. Seasonal timings in maxima and minima of cumulative seagrass cover (**a**) and the population-level effect to seagrass extent (km²) from a 1 unit change in Air Temperature and Direct Normal Radiation (**b**) across 12 seagrass meadows spanning 23° of latitude. Points and error bars show median and 89% confidence intervals for **a** the occurrence of the maxima or minima and **b** the modelled population-level effect. Temperatures ranged from 0 to 25 (°C), and Direct Normal Radiation ranged from 0.0001 to 0.0003 (KW/m²).

captured across our sites with relatively high spatial and temporal resolution. The three main constraints of these data were (1) relatively low spectral resolution, although recent work has shown S2 spectral resolution to be sufficient to distinguish seagrass from other macrobenthic vegetation[23], (2) availability of low tide and cloud-free S2 imagery over the area of interest and (3) the time span of historic data, meaning only 7 years could be consistently assessed (2017–2023). However, for the current analysis, the objective was to create an up-to-date description of inter-tidal seagrass phenology across the North-East Atlantic. Using 7 years of data meant that even in our least data-rich site (Tamar Estuary, $N = 26$), we had similar, if not greater, numbers of images than other assessments of inter-tidal seagrass phenology[44], while our most data-rich site was five times greater (Ria de Aveiro Coastal Lagoon, $N = 129$). These data constitute more recent assessments (2017–2023) than the most comprehensive current analysis of seagrasses available (1880–2016)[40] (these authors also combined sub-tidal and inter-tidal seagrasses). Furthermore, the method could be applied in almost real-time, with potential results within hours of satellite image acquisition and, due to the long-term perspective of the Sentinel-2 mission, our method will make it possible to continuously and consistently monitor seagrass changes across the next few decades and detect possible shifts in seagrass phenology[47].

Seagrass restoration in a changing climate

The valued status of seagrass ecosystems, alongside their general vulnerability to anthropogenic pressures, and subsequent historically and contemporarily depleted distribution, has led to many efforts at restoration[48,49]. Alongside efforts to restore other highly valuable carbon sequestering habitats, such as mangroves and saltmarshes, restoration of inter-tidal seagrass has currently had mixed results[50], yet promising results are being seen with new methodological advances[51]. To be the most successful at restoring these habitats, an understanding of phenology will help restoration practitioners determine the optimal timing for planting to increase the chances of survival and establishment. The timing and rate of seagrass growth will vary with latitude, as shown here, as well as with other influencing factors that remain to be more precisely quantified. For example, Temperature and Direct Radiation showed contrasting effects with latitude. Therefore, it is vitally important to understand these and other local drivers and seasonal patterns to maximise yields from restoration projects. Here, we show that in more northern sites, prolonged times of zero or close to zero, the area of visible above-ground seagrass extent contrasts with dense and extensive summertime maxima. Yet, further south, there are sites where the relative annual change in seagrass extent is far smaller. These distinct differences in phenology mean that restoration projects across these different regions will also need to be equally distinct and designed accordingly to local seasonal dynamics. As global climate change affects both terrestrial and marine vegetation phenology in the North-East Atlantic[52], there is potential that the patterns of phenology seen here will shift, with higher latitude patterns becoming more similar to mid-latitudes, and mid-latitude patterns becoming more similar to low latitudes, often referred to as Tropicalisation (Fig. 5). As shown, northern sites displayed positive relationships with temperature, yet as temperatures increase this may increase desiccation stress[50]. Such phenological shifts could have significant ecological cascading effects, particularly for seagrass herbivores[5,53] and other species closely tied to the seagrass seasonal cycle.
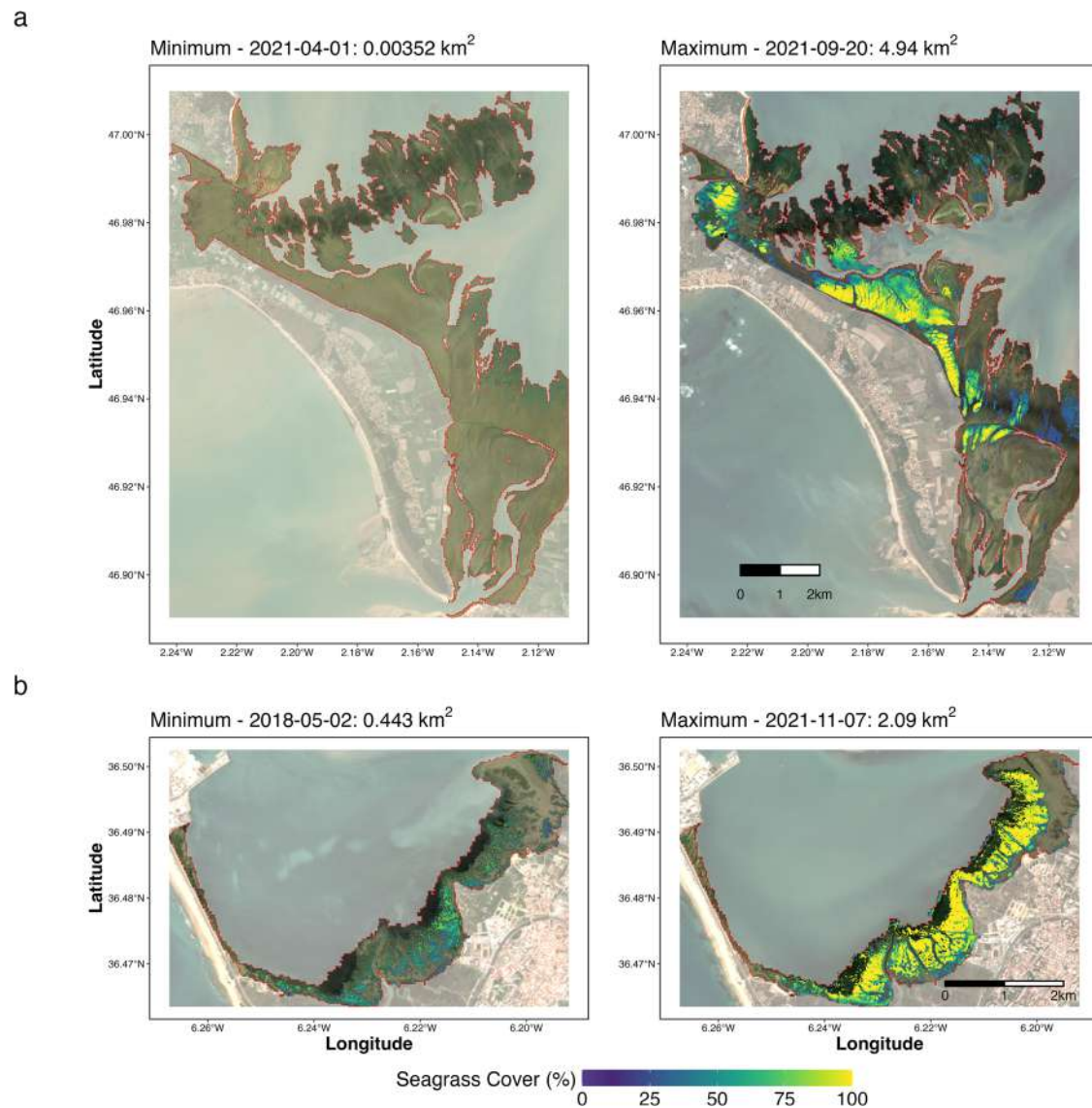
Fig. 4 | Visual Representation of Seasonal Differences in Inter-Tidal Seagrass Cover. Example of distribution at maximum (right) and minimun (left) seagrass cumulative cover from Bourgneuf Bay (**a**), where there is a true minimum of seagrass, and Cádiz Bay (**b**) where seagrass persists all year round. Per pixel percentage seagrass cover (%) is superimposed over a true RGB depiction on the same day. The plotted background Sentinel-2 imagery shows RGB composites downloaded from the Copernicus Portal (https://browser.dataspace.copernicus.eu/). The imagery showed for Bourgneuf Bay **a** were taken on the 2021-09-20, while Cádiz Bay **b** were taken on the 2021-11-07.

Conclusions

This research has provided the first full phenology assessment of intertidal seagrass using 12 sites across a latitudinal gradient at a continental scale using satellite remote sensing and associated environmental drivers. Contrary to established assumptions, we find that there are substantial differences in timing, magnitude and rates of change of seagrass extents in these sites across 23° of latitude along the North-East Atlantic coastline. Northern seagrass sites show the highest rates of change in extent before reaching maximum extent during late boreal summer, being positively related to temperature, while solar radiation showed little to no association. Southern sites show the slowest seasonal rates of change in extent and maximum extent in boreal autumn to winter, displaying little to no relationship with temperature but showing a strong negative relationship with solar radiation. As seagrass conservation, protection and restoration continue to grow and develop on both European and global scales, the method and analysis used here has highlighted how important local information is. More importantly, perhaps, this work shows how lacking the current synoptic mapping of inter-tidal seagrass phenology is. The remote sensing method we have

presented here (ICE CREAMS v1.0) could allow automated near real-time inter-tidal seagrass monitoring. In turn, this would support more effective use of effort and resources for seagrass management; providing up-to-date and accurate estimates of this under-studied blue carbon ecosystem.

Methods
General workflow

To produce data that can be used to accurately and robustly assess the extent of inter-tidal seagrass across continental scales from Sentinel-2 imagery, we followed a two-step process. The first step is to classify inter-tidal habitats and the second is to assess the percentage cover of the area defined as seagrass habitat. These two steps can then be systematically applied to Sentinel-2 imagery to provide information on spatial and temporal inter-tidal seagrass dynamics. The second step in this process (i.e. the computation of seagrass per cent cover from Sentinel-2 surface reflectance) has been tested, validated and applied elsewhere in areas of monospecific seagrass meadows[19]. The first step of the process presents a more complex challenge. To overcome this challenge, we developed a multiclass deep learning Neural Network (NN)
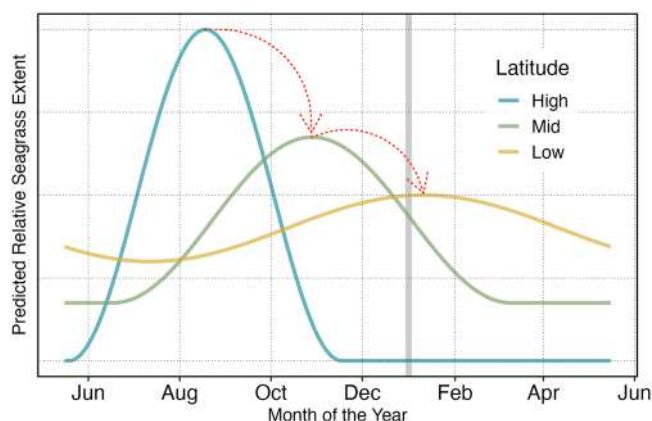
Fig. 5 | Climate change potentially altering Phenology. Theoretical diagram of inter-tidal seagrass phenology across three different latitudes (high, medium and low). The dotted arrows show the theoretical effect of global climate change on shifting phenology of higher latitude seagrass meadows to be more similar to lower latitude seagrass meadows. The vertical shaded line shows January 1st.

classifier called the Intertidal Classification of Europe: Categorising Reflectance of Emerged Areas of Marine vegetation with Sentinel-2 (ICE CREAMS v1.0). An NN classifier was selected as they are effective at multiclass classification tasks with high numbers of features, non-linear relationships and collinearity of features[54]. NN classifiers can also be systematically deployed in a wide variety of computing languages and frameworks[55]. To build the ICE CREAMS model, training data were derived from high spatial resolution drone imagery that coincided spatially and temporally with Sentinel-2 imagery (exact pixels within 15 days), the model was then validated using independent photo quadrat and RGB drone imagery that likewise coincided spatially and temporally with Sentinel-2 imagery (Fig. 6). The ICE CREAMS model was then applied to all low tide, cloud-free Sentinel-2 imagery from 2017 to 2023 available from 12 known inter-tidal seagrass meadows across Western Europe and Northern Africa[6,19,56–63] to provide habitat classification at the 10 m resolution. Dynamics of inter-tidal seagrass extent were assessed by converting each seagrass pixel into Seagrass Percentage Cover[19].

Neural network inter-tidal classifier
Training data. High classification accuracy at Sentinel-2's spectral resolution has previously been shown for Class level inter-tidal habitats[23], so data were labelled at the Class level for vegetated habitats alongside other non-vegetated habitat types. Pixels were labelled into 9 classes: Bare Sand, Bare Mud, Ulvophyceae (green macroalgae), Magnoliopsida (seagrass), Microphytobenthos (unicellular photosynthetic eukaryotes and cyanobacteria forming biofilms at the sediments surface during low tide), Mixed-Rocks with associated Phaeophyceae (brown macroalgae), Rhodophyceae (red macroalgae), Xanthophyceae (yellow-green macroalgae) and Water. Due to the heterogeneous nature of inter-tidal habitats, both spatially and temporally, labelled data need to align spatially and temporally to available Sentinel-2 imagery. Therefore, training data were collated across a range of methods to account for this difference in spatial and temporal variability of habitats. For classes that show greater variability in their spatial extent over time: drone imagery-derived data were used. For classes that show spatial fidelity over time: additional data were collected, alongside drone acquisition, through visual inspection of Sentinel-2 imagery.

Drone acquisition
To adequately cover the expected spectral variability of inter-tidal habitat classes that occur across the North-East Atlantic coast, drone imagery was taken from multiple sites in Western Europe (Auray Estuary, Morbihan Gulf, Bourgneuf Bay and Ria de Aveiro Coastal Lagoon: Fig. 7). Drone imagery was acquired at two different flight altitudes (12 and 120 m) meaning pixel sizes were either 8 or 80 mm, allowing the classification of habitats at high spatial resolution. In total, these drone images covered over 4 km^2 of inter-tidal habitats.

Visual inspection
To increase the balance between classes, pixels of some classes, such as bare muds and sands, sediments containing high abundances of microphytobenthos, as well as hard substrates covered by vegetation, were added to the training dataset (Fig. 7). These pixels were selected through visual inspection of spectral signatures, true colour RGB and false colour imagery derived from Sentinel-2 accessed and visualised through the Copernicus data portal.

Alignment of habitat and sentinel-2 imagery
All labelled data were aggregated (majority class) to the 10 m resolution of Sentinel-2, and then all Level-2A Sentinel-2 A/B images that coincided spatially and temporally (±15 days) with these labelled were downloaded from the Copernicus data portal. Level-2A data have already been atmospherically corrected using the Sen2Cor processing algorithm[64], and are distributed as bottom-of-atmosphere (BOA) reflectance. Manual inspection of RGB true colour was used to select cloud-free and low-tide Sentinel-2 images to remove any unusable images.

Pre-processing
All 12 bands of Sentinel-2 were resampled to 10 m resolution and standardised following a Min-Max Standardisation[22,23]. Furthermore, normalised difference vegetation index (NDVI) and normalised difference water index (NDWI) were calculated for each pixel from the BOA Sentinel-2 reflectance values:

$$NDVI = \frac{R(832) - R(664)}{R(832) + R(664)} \tag{1}$$

$$NDWI = \frac{R(560) - R(832)}{R(560) + R(832)} \tag{2}$$

with $R(560)$, $R(664)$ and $R(832)$ being the green (Sentinel-2 band centred on 560 nm), red (Sentinel-2 band centred on 664 nm) and near-infra-red (Sentinel-2 band centred on 832 nm) spectral domains respectively. Within the Magnoliopsida class, there is a maximum diversity of three species *Nanozostera noltei*, *Zostera marina* and *Cymodocea nodosa*, although *Nanozostera noltei* was the dominant species across most inter-tidal sites assessed. This created a labelled tabular dataset of 338,526 rows with classes in one column and features in 26 others: 12 BOA reflectance columns, 12 Min-Max standardised reflectance columns, and 2 columns for NDVI and NDWI.

Model building
Labelled pixels consisting of all 26 features were used to train a deep learning neural network tabular learner from the FastAI framework in Python v3[55,65]. The model consisted of 2 hidden layers with 26,761 trainable parameters and was fine-tuned across 20 epochs to minimise cross entropy loss using the ADAptive Moment estimation (ADAM) optimiser. The final within-sample error rate was 0.0365. The ICE CREAMS model provided a classification for each pixel, based on the greatest probability class.

Validation data
To ensure validation of the ICE CREAMS model was independent of model building, several methods were employed to generate validation data. Field campaigns were carried out by taking geo-located photo quadrats. These photo quadrats were taken within the Tagus Estuary and Ria de Aveiro Coastal Lagoon (Portugal[66]), and Bourgneuf Bay and Ria D'Etel (France). Further validation data were collected through Red Green Blue (RGB) drone imagery, taken within two estuaries in the UK (Tamar and Kingsbridge) and a bay in Spain (Cádiz: Fig. 7). As with training data, labelled validation data were aggregated (majority class) to the 10 m resolution of Sentinel-2, then all Level-2A Sentinel-2 A/B images that coincided spatially and temporally (±15 days) with these labelled were downloaded from the Copernicus data
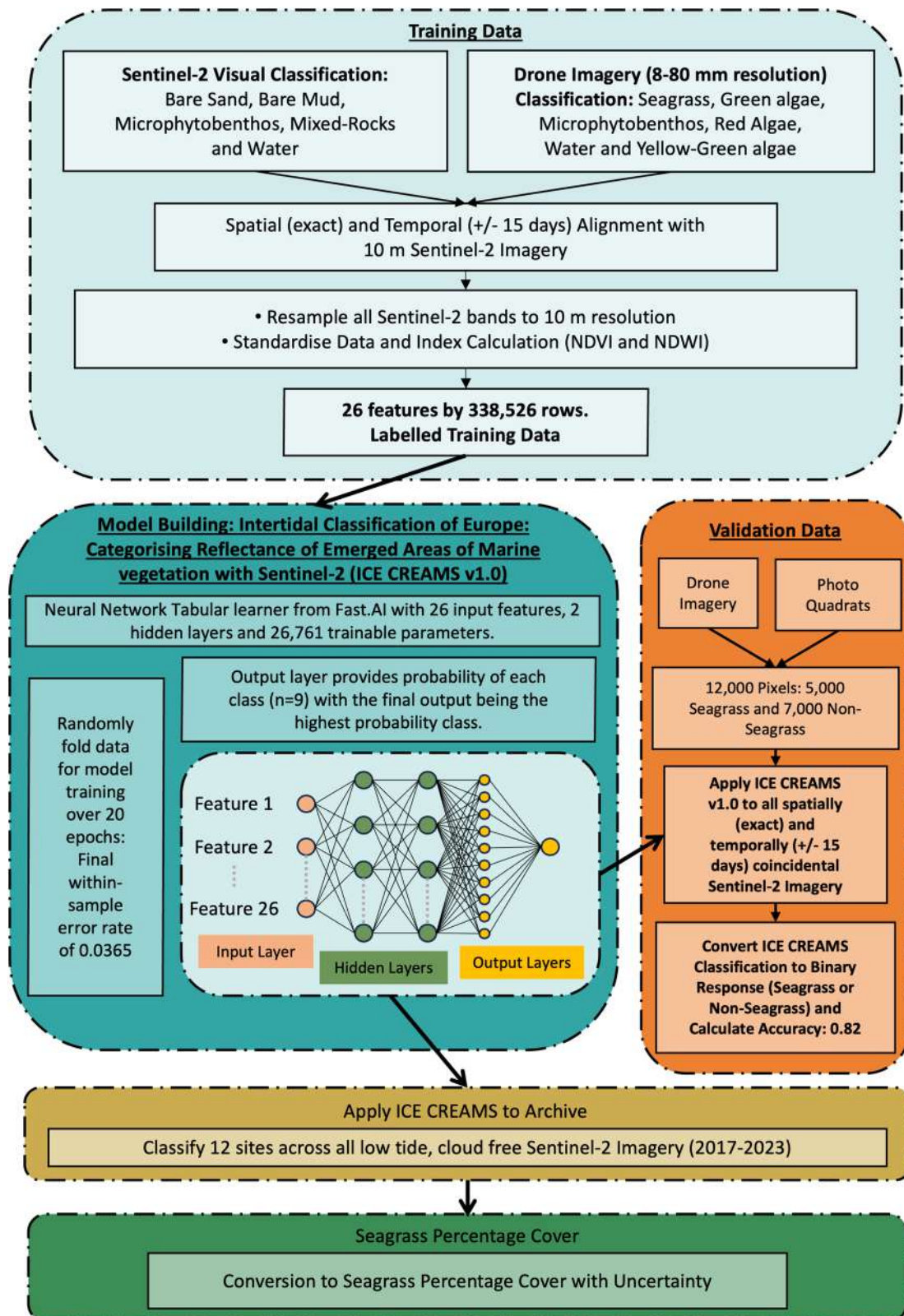
Fig. 6 | Methodology Employed to Apply ICE CREAMS. Flow chart showing the process of Creating the Intertidal Classification of Europe: categorising reflectance of emerged areas of marine vegetation with Sentinel-2 (ICE CREAMS v1.0) model.

portal. The ICE CREAMS model was applied to these Sentinel-2 images that aligned spatially and temporally with the validation data. The model predictions were then compared to the validation data labels. Global model accuracy (G_a) was calculated across all validation data as the binary presence or absence of seagrass across ~12,000 Sentinel-2 pixels: ~5000 Seagrass

Pixels and ~7000 Non-Seagrass Pixels:

$$G_a = \frac{n_{TP} + n_{TN}}{n_{TP} + n_{TN} + n_{FP} + n_{FN}} \qquad (3)$$
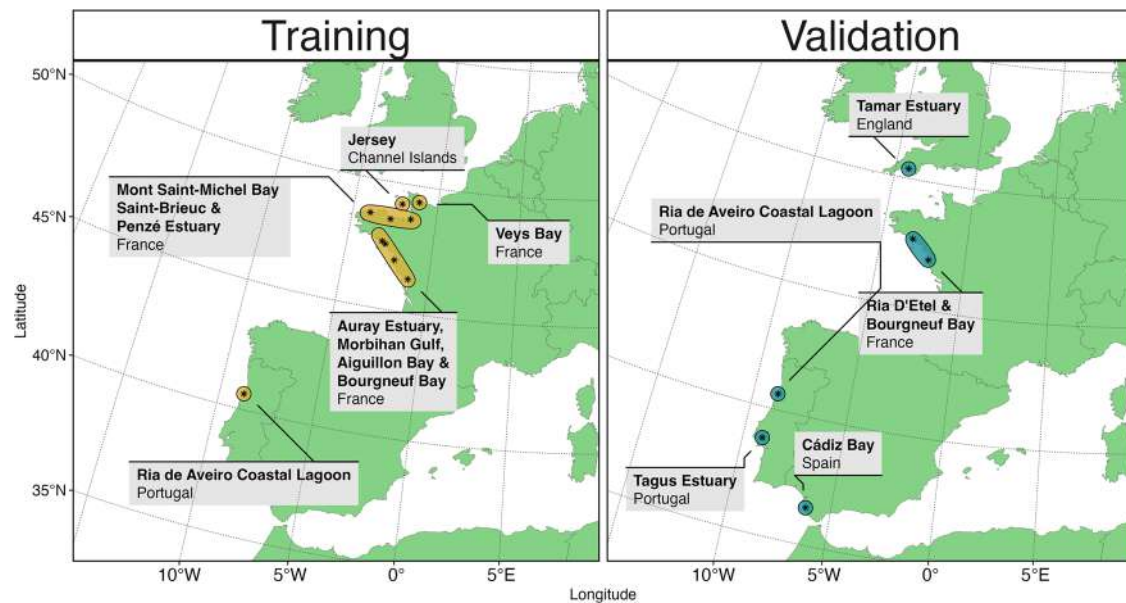
Fig. 7 | Location of all in situ data taken from across Europe for ICE CREAMS model. The left hand panel shows sites used for model training, while the right hand panel shows sites used for validation.

Fig. 8 | Accuracy of ICE CREAMS model. Binary validation of ICE CREAMS neural network showing the proportion of total samples in an agreement between truth and predicted seagrass and non-seagrass pixels, with a number of total pixels within each grid cell. External labels with numbers show within-class sensitivity and specificity and the positive predicted value (PPV) and negative predicted value (NPV).
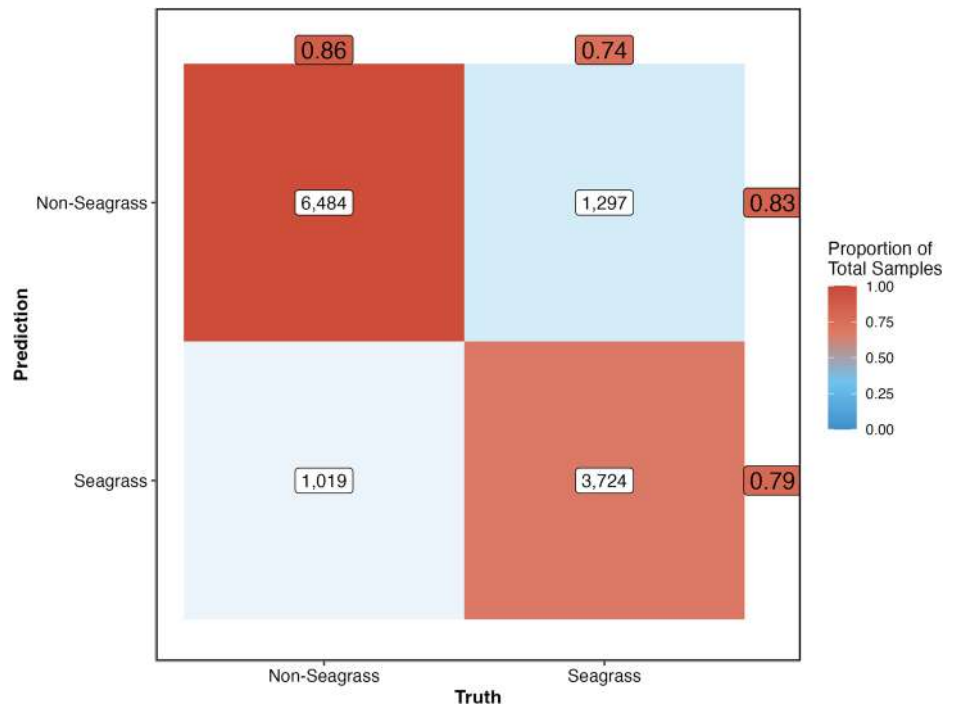
where n_{TP} is the number of True Positives, n_{TN} the number of True Negatives, n_{FP} the number of False Positives and n_{FN} the number of False Negatives. The ICE CREAMS model achieved a G_a of 0.82 (Fig. 8). Non-Seagrass pixels contained a mixture of the non-seagrass classes with ~1000 green macroalgae, ~3000 bare sand and mud, ~2000 microphytobenthos and ~1000 Mixed-Rocks with associated brown macroalgae.

Site selection. Twelve sites were selected across ~23° latitude along the North Western Atlantic Coast of Europe and Africa (Fig. 7). Sites were selected where known inter-tidal seagrass meadows were present[6,19,56–63]. For each site, all cloud-free, low-tide Sentinel-2 L2A images were selected from the Sentinel-2 long term archive (LTA: Table 1). A mask was used to

isolate only pixels within the inter-tidal area[43], then the Neural Network model was applied to classify inter-tidal habitats within each 100 m² pixel.

Inter-tidal seagrass cover. The model provided a classification for each pixel based on the greatest probability class. For every pixel where seagrass was predicted, the seagrass percentage cover (SPC) was calculated[19]. Following this method only SPC values above 20% were selected for analysis:

$$SPC = 172.06 * \text{NDVI} - 22.18$$

As each pixel is 100 m² the summed SPC within each site could be considered the total area covered by seagrass in m^2 per image. Pixels

Table 1 | Number of images analysed by location and year as well as total images analysed across all years

Location	Country	Latitude (°N)	Longitude (°E)	Area (km²)	2017	2018	2019	2020	2021	2022	2023	Total
					Number of images analysed							
Merja Zerga	Morroco	34.8	−6.273	11	8	16	13	20	20	14	12	103
Cádiz Bay	Spain	36.5	−6.226	6	3	15	14	12	15	11	14	84
Tagus Estuary	Portugal	38.7	−9.025	51	7	7	9	8	9	11	9	60
Ria de Aveiro Coastal Lagoon	Portugal	40.7	−8.746	14	10	20	20	14	18	24	23	129
Santander Bay	Spain	43.4	−3.795	7	1	6	7	7	4	4	10	39
Marennes-Oléron Bay	France	46.0	−1.154	80	3	11	10	5	11	4	3	47
Bourgneuf Bay	France	47.0	−2.098	46	3	15	11	14	17	16	8	84
Tamar Estuary	England	50.0	−4.191	3	0	3	2	4	9	4	4	26
Milford Haven	Wales	52.0	−5.050	5	4	9	3	14	6	8	7	51
Beltringharder Koog	Germany	54.6	8.608	352	5	21	11	9	12	12	11	81
Strangford Lough	Northern Ireland	55.0	−5.587	23	5	9	5	5	11	10	9	54
Cromarty Firth	Scotland	57.6	−4.069	8	1	10	7	3	1	5	10	37

displaying less than 0.25 NDVI were removed from analysis as macrovegetation was not deemed to be the dominant class, this equated to an SPC cut off of ~20. The uncertainty for each image (τ) was calculated as the inverse of the mean of the per pixel probabilities from the classification model divided by the global accuracy (G_a) of the model when applied to validation data:

$$\tau = \frac{1 - \bar{p}}{G_a} \tag{4}$$

Environmental driver data. Two environmental datasets were selected to provide insight into drivers of seagrass extent. Monthly Air Temperature and Direct Normal Radiation from 2017 to 2023 were downloaded from International Energy Agency and Copernicus Climate Change Service repository[67]. Each inter-tidal seagrass extent value was assigned the Temperature (°C) and direct normal radiation (W/m²) from the month immediately preceding it and from its immediate spatial extent.

Statistical analysis

Phenology assessment. A multilevel general additive model (GAM)[68] was used to assess phenology of seagrass extent across our sites, model parameters were estimated within a bayesian framework using the 'brms' and 'RStan' packages in R to leverage the Stan language[69–72]. Observed total seagrass cover ($E*_i$) and its uncertainty (τ_i) were modelled as a function of Day of the Year with a cyclic basis spline ($f(t_i)$) across Locations (ρ) with Year (Y) as a random factor. The response variable was modelled assuming a Student-t distribution, with weakly informative priors (Student-T(3,0,2.5)). Model parameters were estimated using Markov Chain Monte Carlo (MCMC) sampling, with 4 chains of 5000 iterations and a warm-up of 500.

$$
\begin{aligned}
E*_i &\sim Student(E_i, \tau_i) \\
E_i &\sim Student(\mu_i, \sigma_i) \\
\mu_i &= a_{Y[i]} + f(t_i) : \rho \\
a_{Y[i]} &\sim Student(\bar{a}, \delta) \\
\bar{a} &\sim Student(3, 0, 2.5) \\
f(t_i) : \rho &\sim Student(3, 0, 2.5) \\
\delta &\sim Student(3, 0, 2.5) \\
\sigma &\sim Student(3, 0, 2.5)
\end{aligned} \tag{5}
$$

Phenology metrics

To assess the differences in seagrass extent phenology across locations, 2000 posterior predictive draws were taken from the model. Phenology metrics were taken from these modelled phenology patterns, with maxima and minima being the maximum and minimum values of the median prediction across the draws. Timing of maximum and minimum extent was estimated as the maximum and minimum for the median prediction across the 2000 draws, with uncertainty in the day of the year taken as the 89% Confidence Interval at that maximum/minimum value. The rate of change in seagrass extent was taken as the first derivative of the model, using a sliding window of 7 days and reported as km² per week (km² w⁻¹).

Environmental drivers. A multilevel general additive model (GAM)[68] was used to assess environmental drivers of seagrass extent across our sites, model parameters were estimated within a bayesian framework using the 'brms' and 'RStan' packages in R to leverage the Stan language[69–72]. Observed total seagrass cover ($E*_i$) and its uncertainty (τ_i) were modelled as a function of monthly averaged temperature with a single knot ($f(AT_i)$) across locations (ρ) and log transformed monthly averaged direct normal radiation with a single knot ($f(AS_i)$) across locations (ρ) with year (Y) as a random factor. The response variable was modelled assuming a Student-t distribution, with weakly informative priors (Student-t(3,0,2.5)). Model parameters were estimated using Markov Chain Monte Carlo (MCMC) sampling, with 4 chains of 5000 iterations and a warm-up of 500.

$$
\begin{aligned}
E*_i &\sim Student(E_i, \tau_i) \\
E_i &\sim Student(\mu_i, \sigma_i) \\
\mu_i &= a_{Y[i]} + f(AT_i) : \rho + f(AS_i) : \rho \\
a_{Y[i]} &\sim Student(\bar{a}, \delta) \\
\bar{a} &\sim Student(3, 0, 2.5) \\
f(AT_i) : \rho &\sim Student(3, 0, 2.5) \\
f(AS_i) : \rho &\sim Student(3, 0, 2.5) \\
\delta &\sim Student(3, 0, 2.5) \\
\sigma &\sim Student(3, 0, 2.5)
\end{aligned} \tag{6}
$$

Environmental effects. The population-level effect estimates and 89% confidence intervals were retrieved from the model to compare the effect of temperature and direct normal radiation within each location.

Reporting summary

Further information on research design is available in the Nature Portfolio Reporting Summary linked to this article.

References

1. Cullen-Unsworth, L. C. et al. Seagrass meadows globally as a coupled social–ecological system: implications for human wellbeing. *Mar. Pollut. Bull.* **83**, 387–397 (2014).
2. Dewsbury, B. M., Bhat, M. & Fourqurean, J. W. A review of seagrass economic valuations: gaps and progress in valuation approaches. *Ecosyst. Serv.* **18**, 68–77 (2016).
3. Whitfield, A. K. The role of seagrass meadows, mangrove forests, salt marshes and reed beds as nursery areas and food sources for fishes in estuaries. *Rev. Fish. Biol. Fish.* **27**, 75–110 (2017).
4. Unsworth, R. K. F., Nordlund, L. M. & Cullen-Unsworth, L. C. Seagrass meadows support global fisheries production. *Conserv. Lett.* **12**, 1–8 (2019).
5. Zoffoli, M. L. et al. Remote sensing in seagrass ecology: coupled dynamics between migratory herbivorous birds and intertidal meadows observed by satellite during four decades. *Remote Sens. Ecol. Conserv.* **9**, 420–433 (2022).
6. Sousa, A. I., Silva, J. F., da, Azevedo, A. & Lillebø, A. I. Blue carbon stock in *Zostera noltei* meadows at ria de aveiro coastal lagoon (portugal) over a decade. *Sci. Rep.* **9**, 14387 (2019).
7. Paul, M. & Amos, C. Spatial and seasonal variation in wave attenuation over *Zostera noltii*. *J. Geophys. Res.* **116**, 1–16 (2011).
8. Orth, R. J. et al. Restoration of seagrass habitat leads to rapid recovery of coastal ecosystem services. *Sci. Adv.* **6**, eabc6434 (2020).
9. Turschwell, M. P. et al. Anthropogenic pressures and life history predict trajectories of seagrass meadow extent at a global scale. *Proc. Natl Acad. Sci. USA* **118**, e2110802118 (2021).
10. Cardoso, P. et al. Dynamic changes in seagrass assemblages under eutrophication and implications for recovery. *J. Exp. Mar. Biol. Ecol.* **302**, 233–248 (2004).
11. Garmendia, J. M. et al. Estimated footprint of shellfishing activities in *Zostera noltei* meadows in a northern Spain estuary: lessons for management. *Estuar. Coast. Shelf Sci.* **254**, 107320 (2021).
12. Momota, K. & Hosokawa, S. Potential impacts of marine urbanization on benthic macrofaunal diversity. *Sci. Rep.* **11**, 1–12 (2021).
13. Duarte, C. M., Losada, I. J., Hendriks, I. E., Mazarrasa, I. & Marbà, N. The role of coastal plant communities for climate change mitigation and adaptation. *Nat. Clim. Change* **3**, 961–968 (2013).
14. McKenzie, L. J. et al. The global distribution of seagrass meadows. *Environ. Res. Lett.* **15**, 074041 (2020).
15. Macreadie, P. I. et al. Blue carbon as a natural climate solution. *Nat. Rev. Earth Environ.* **2**, 826–839 (2021).
16. Veettil, B. K. et al. Opportunities for seagrass research derived from remote sensing: a review of current methods. *Ecol. Indic.* **117**, 106560 (2020).
17. Zoffoli, M. L. et al. Decadal increase in the ecological status of a north-Atlantic intertidal seagrass meadow observed with multi-mission satellite time-series. *Ecol. Indic.* **130**, 108033 (2021).
18. Lizcano-Sandoval, L. et al. Seagrass distribution, areal cover, and changes (1990–2021) in coastal waters off west-central Florida, USA. *Estuar. Coast. Shelf Sci.* https://doi.org/10.1016/j.ecss.2022.108134 (2022).
19. Zoffoli, M. L. et al. Sentinel-2 remote sensing of *Zostera noltei*-dominated intertidal seagrass meadows. *Remote Sens. Environ.* **251**, 112020 (2020).
20. Spectral reflectance of the seagrasses. *Thalassia testudinum*, *Halodule wrightii*, *Syringodium filiforme* and five marine algae. *Int. J. Remote Sens.* **28**, 1487–1501 (2007).
21. Olmedo-Masat, O. M., Paula Raffo, M., Rodríguez-Pérez, D., Arijón, M. & Sánchez-Carnero, N. How far can we classify macroalgae remotely? An example using a new spectral library of species from the South West Atlantic (Argentine Patagonia). *Remote Sens.* **12**, 1–33 (2020).
22. Douay, F., Verpoorter, C., Duong, G., Spilmont, N. & Gevaert, F. New hyperspectral procedure to discriminate intertidal macroalgae. *Remote Sens.* **14**, 346 (2022).
23. Davies, B. F. R. et al. Multi-and hyperspectral classification of soft-bottom intertidal vegetation using a spectral library for coastal biodiversity remote sensing. *Remote Sens. Environ.* **290**, 113554 (2023).
24. Traganos, D. et al. Spatially explicit seagrass extent mapping across the entire Mediterranean. *Front. Mar. Sci.* **9**, 871799 (2022).
25. Philippart, C. Seasonal variation in growth and biomass of an intertidal *Zostera noltii* stand in the Dutch Wadden sea. *Neth. J. Sea Res.* **33**, 205–218 (1995).
26. Vermaat, J. E. & Verhagen, F. C. Seasonal variation in the intertidal seagrass *Zostera noltii* hornem.: coupling demographic and physiological patterns. *Aquat. Bot.* **52**, 259–281 (1996).
27. De Los Santos, C. B., Brun, F. G., Bouma, T. J., Vergara, J. J. & Pérez-Lloréns, J. L. Acclimation of seagrass *Zostera noltii* to co-occurring hydrodynamic and light stresses. *Mar. Ecol. Prog. Ser.* **398**, 127–135 (2010).
28. Costa, V., Serôdio, J., Lillebø, A. I. & Sousa, A. I. Use of hyperspectral reflectance to non-destructively estimate seagrass *Zostera noltei* biomass. *Ecol. Indic.* **121**, 107018 (2021).
29. Soissons, L. M. et al. Latitudinal patterns in European seagrass carbon reserves: influence of seasonal fluctuations versus short-term stress and disturbance events. *Front. Plant Sci.* **9**, 88 (2018).
30. Soissons, L. M. et al. Seasonal and latitudinal variation in seagrass mechanical traits across Europe: the influence of local nutrient status and morphometric plasticity. *Limnol. Oceanogr.* **63**, 37–46 (2018).
31. Ankel, M., Rubal, M., Veiga, P., Sampaio, L. & Guerrero-Meseguer, L. Reproductive cycle of the seagrass *Zostera noltei* in the ria de aveiro lagoon. *Plants* **10**, 2286 (2021).
32. Fouw et al. A facultative mutualism facilitates European seagrass meadows. *Ecography* https://doi.org/10.1111/ecog.06636 (2023).
33. Sousa, A. I. et al. Effect of spatio-temporal shifts in salinity combined with other environmental variables on the ecological processes provided by *Zostera noltei* meadows. *Sci. Rep.* **7**, 1336 (2017).
34. Clausen, K. K., Krause-Jensen, D., Olesen, B. & Marbà, N. Seasonality of eelgrass biomass across gradients in temperature and latitude. *Mar. Ecol. Prog. Ser.* **506**, 71–85 (2014).
35. Duarte, C. M. Temporal biomass variability and production/biomass relationships of seagrass communities. *Mar. Ecol. Prog. Ser. Oldendorf* **51**, 269–276 (1989).
36. Ito, M. A., Lin, H.-J., Connor, M. I. & Nakaoka, M. Large-scale comparison of biomass and reproductive phenology among native and non-native populations of the seagrass *Zostera japonica* japonica. *Mar. Ecol. Prog. Ser.* **675**, 1–21 (2021).
37. Zhang, X., Friedl, M. A., Schaaf, C. B. & Strahler, A. H. Climate controls on vegetation phenological patterns in northern mid-and high latitudes inferred from MODIS data. *Glob. Change Biol.* **10**, 1133–1145 (2004).
38. Waycott, M. et al. Accelerating loss of seagrasses across the globe threatens coastal ecosystems. *Proc. Natl Acad. Sci. USA* **106**, 12377–12381 (2009).
39. Los Santos et al. Recent trend reversal for declining European seagrass meadows. *Nat. Commun.* **10**, 3356 (2019).
40. Dunic, J. C., Brown, C. J., Connolly, R. M., Turschwell, M. P. & Côté, I. M. Long-term declines and recovery of meadow area across the world's seagrass bioregions. *Glob. Change Biol.* **27**, 4096–4109 (2021).

41. Pereira, H. M. et al. Essential biodiversity variables. *Science* **339**, 277–278 (2013).

42. Muller-Karger, F. E. et al. Satellite sensor requirements for monitoring essential biodiversity variables of coastal ecosystems. *Ecol. Appl.* **28**, 749–760 (2018).

43. Murray, N. J. et al. The global distribution and trajectory of tidal flats. *Nature* **565**, 222–225 (2019).

44. Clemente, K. J. E., Thomsen, M. S. & Zimmerman, R. C. The vulnerability and resilience of seagrass ecosystems to marine heatwaves in New Zealand: a remote sensing analysis of seascape metrics using PlanetScope imagery. *Remote Sens. Ecol. Conserv.* **9**, 803–819 (2023).

45. Gorelick, N. et al. Google Earth Engine: planetary-scale geospatial analysis for everyone. *Remote Sens. Environ.* **202**, 18–27 (2017).

46. Bargain, A. et al. Seasonal spectral variation of *Zostera noltii* and its influence on pigment-based vegetation indices. *J. Exp. Mar. Biol. Ecol.* **446**, 86–94 (2013).

47. Löscher, A. et al. The ESA sentinel next-generation land & ocean optical imaging architectural study, an overview. *Sens. Syst. Gener. Satell. XXIV* **11530**, 15–26 (2020).

48. Zhang, X. et al. Temporal pattern in biometrics and nutrient stoichiometry of the intertidal seagrass *Zostera japonica* and its adaptation to air exposure in a temperate marine lagoon (china): implications for restoration and management. *Mar. Pollut. Bull.* **94**, 103–113 (2015).

49. Mokumo, M. F., Adams, J. B. & Heyden, S. von der. Investigating transplantation as a mechanism for seagrass restoration in South Africa. *Restor. Ecol.* https://doi.org/10.1111/rec.13941 (2023).

50. Suykerbuyk, W. et al. Unpredictability in seagrass restoration: Analysing the role of positive feedback and environmental stress on *Zostera noltii* transplants. *J. Appl. Ecol.* **53**, 774–784 (2016).

51. Gräfnings, M. L. et al. Optimizing seed injection as a seagrass restoration method. *Restor. Ecol.* **31**, e13851 (2023).

52. González Taboada, F. & Anadón, R. Seasonality of north Atlantic phytoplankton from space: Impact of environmental forcing on a changing phenology (1998–2012). *Glob. Change Biol.* **20**, 698–712 (2014).

53. Longo, G. O. Seagrass vulnerability to tropicalization-induced herbivory. *Nat. Ecol. Evolut.* **8**, 600–601 (2024).

54. Pichler, M. & Hartig, F. Machine learning and deep learning—a review for ecologists. *Methods Ecol. Evolut.* **14**, 994–1016 (2023).

55. Howard, J. & Gugger, S. Fastai: a layered API for deep learning. *Information* **11**, 108 (2020).

56. Potouroglou, M. et al. The sediment carbon stocks of intertidal seagrass meadows in Scotland. *Estuar. Coast. Shelf Sci.* **258**, 107442 (2021).

57. Dolch, T., Buschbaum, C. & Reise, K. Persisting intertidal seagrass beds in the Northern Wadden Sea since the 1930s. *J. Sea Res.* **82**, 134–141 (2013).

58. Wilkes, R. et al. Intertidal seagrass in Ireland: pressures, WFD status and an assessment of trace element contamination in intertidal habitats using *Zostera noltii*. *Ecol. Indic.* **82**, 117–130 (2017).

59. Bertelli, C. M., Robinson, M. T., Mendzil, A. F., Pratt, L. R. & Unsworth, R. K. Finding some seagrass optimism in Wales, the case of *Zostera noltii*. *Mar. Pollut. Bull.* **134**, 216–222 (2018).

60. Green, A. E., Unsworth, R. K., Chadwick, M. A. & Jones, P. J. Historical analysis exposes catastrophic seagrass loss for the United Kingdom. *Front. Plant Sci.* **12**, 629962 (2021).

61. Calleja, F., Galván, C., Silió-Calzada, A., Juanes, J. A. & Ondiviela, B. Long-term analysis of *Zostera noltii*: a retrospective approach for understanding seagrasses' dynamics. *Mar. Environ. Res.* **130**, 93–105 (2017).

62. Martins, D., Alves da Silva, A., Duarte, J., Canário, J. & Vieira, G. Changes in vessel traffic disrupt tidal flats and saltmarshes in the Tagus estuary, Portugal. *Estuar. Coasts* **46**, 1141–1156 (2023).

63. Benmokhtar, S. et al. Monitoring the spatial and interannual dynamic of *Zostera noltii*. *Wetlands* **43**, 43 (2023).

64. Main-Knorn, M. et al. Sen2Cor for sentinel-2. in *Image and signal processing for remote sensing XXIII* vol. 10427 37–48 (SPIE, 2017).

65. Van Rossum, G. & Drake, F. L. *Python 3 Reference Manual*. (CreateSpace, 2009).

66. Davies, B. F. R. et al. Benthic intertidal vegetation from the Tagus estuary and Aveiro lagoon. Version 1.6. Université de nantes. Sampling event dataset https://doi.org/10.15468/n4ak6x accessed via GBIF.org. (2023).

67. IEA & CMCC. Weather for energy tracker, license: Creative commons CC BY-NC-ND 3.0 IGO. Dataset https://www.iea.org/data-and-statistics/data-tools/weather-climate-and-energy-tracker?tab=weather+for+energy+tracker accessed via iea.org. (2024).

68. Wood, S. N. *Generalized Additive Models: an Introduction With r*. (Chapman; Hall/CRC, 2017).

69. Bürkner, P.-C. Bayesian item response modeling in R with brms and Stan. *J. Stat. Softw.* **100**, 1–54 (2021).

70. Stan Development Team. *RStan: The R interface to Stan* (2018).

71. Carpenter, B. et al. Stan: a probabilistic programming language. *J. Stat. Softw.* **76**, 1 (2017).

72. R Core Team. *R: A Language and Environment for Statistical Computing*. (R Foundation for Statistical Computing, 2023).

Acknowledgements

Competing interests

The authors declare no competing interests.

Additional information

Supplementary information The online version contains supplementary material available at https://doi.org/10.1038/s43247-024-01543-z.

Correspondence and requests for materials should be addressed to Bede Ffinian Rowe Davies.

Peer review information *Communications Earth & Environment* thanks Stuart Phinn and the other, anonymous, reviewer(s) for their contribution to the peer review of this work. Primary Handling Editors: Christopher Cornwall, Alireza Bahadori and Clare Davis. A peer review file is available.

Reprints and permissions information is available at http://www.nature.com/reprints